PCCP

PAPER

View Article Online
View Journal | View Issue

Check for updates

Cite this: *Phys. Chem. Chem. Phys.*, 2018, **20**, 14024

Lattice thermal conductivity of monolayer AsP from first-principles molecular dynamics†

Yajing Sun, [a] Zhigang Shuai [abc] and Dong Wang *[a]

Few-layered arsenic–phosphorus alloys, $As_xP_{(1-x)}$, with a puckered structure have been recently synthesized and demonstrated with fully tunable band gaps and optical properties. It is predicted that the carrier mobility of monolayer AsP compounds is even higher than that of black phosphorene (b-P). The anisotropic and orthogonal electrical and thermal transport properties of the puckered group VA elements make them intriguing materials for thermoelectric applications. Herein, we investigated the thermal transport properties of AsP based on first-principles molecular dynamics and the Boltzmann transport equation. We reveal that monolayer AsP with three different chemical structures possesses thermal conductivities lower than b-P, but with increased anisotropy. Further, these structures behave profoundly different on heat conduction. This can be attributed to the distinct low-frequency optical modes associated with their bonding nature. Our results highlight the impact of atomic arrangement on the thermal conductivity of AsP, and the structure–property relationship established may guide the fabrication of thermoelectric materials *via* the engineered alloying method.

Received 22nd March 2018,
Accepted 24th April 2018

DOI: 10.1039/c8cp01840e

rsc.li/pccp

Published on 25 April 2018. Downloaded by Tsinghua University on 6/28/2018 3:59:49 AM.

1. Introduction

Two-dimensional (2D) layered materials, including graphene, hexagonal boron nitride (h-BN), and transition metal dichalcogenides (TMDCs), have attracted significant attention due to their unique electronic, optical, and mechanical properties.[1–7] One of the newest members to the family of 2D layered materials is group VA elements.[8] Black phosphorene (b-P), arsenene, and antimonene have sizeable band gaps ranging from 1 to 2.5 eV, which depend strongly on the number of layers and can be easily tuned by strains.[9–13] Moreover, both theoretical calculations and experimental measurements indicate that black phosphorene has mobility of the order of 10^3 cm^2 V^{-1} s^{-1}, whereas the carrier mobilities of arsenene and antimonene are of the order of 10^1–10^2 cm^2 V^{-1} s^{-1} due to large deformation potential constants.[9,14–16] These properties make the 2D group VA elements promising for applications in next-generation nanoelectronic, optoelectronic, and thermoelectric devices.[10,16–18] More interestingly, charge and thermal transport in the puckered group VA materials are highly anisotropic, and their preferential transport directions are orthogonal to each other; this definitely benefits the thermoelectric conversion.

Alloying has been demonstrated as an efficient strategy for tuning the physical properties of materials. Arsenic was even incorporated into black phosphorous *via* a high-pressure process to achieve superconducting properties at around 10 K.[19] Recent theoretical studies predict that the 1 : 1 b-AsP monolayer possesses extremely high charge mobility, almost three times that of b-P.[20,21] Moreover, alloying usually decreases the lattice thermal conductivity of materials due to enhanced phonon scatterings. Similar to the cases in Si–Ge and Bi–Sb systems, alloying was found to significantly reduce the thermal conductivity.[22,23] Moreover, isoelectronic substitution of Si by Ge can tune the anisotropy of thermal conductivity.[24] Compared to b-P, AsP may have higher mobility and lower lattice thermal conductivity; this demonstrates the potential of AsP as an efficient thermoelectric material.

In this study, we focused on the phonon properties of single-layered AsP compounds and explored how chemical structures influence the lattice thermal conductivities and anisotropy. Although there are theoretical calculations indicating that buckled AsP is more stable,[25] we have chosen puckered AsP (such as b-P) for our study since puckered $As_xP_{(1-x)}$ alloys have been recently prepared experimentally in few layers.[26] Typically, three types of chemical structures exist for single-layered AsP. By performing first-principles calculations, we showed that all these structures might be stable in monolayers and possess thermal conductivities lower than those of b-P, but with higher anisotropy. We have demonstrated that different thermal

[a] *MOE Key Laboratory of Organic Opto Electronics and Molecular Engineering, Department of Chemistry, Tsinghua University, Beijing 100084, P. R. China. E-mail: dong913@tsinghua.edu.cn*
[b] *Key Laboratory of Organic Solids, Beijing National Laboratory for Molecular Science (BNLMS), Institute of Chemistry, Chinese Academy of Sciences, Beijing 100190, P. R. China*
[c] *Collaborative Innovation Center of Chemistry for Energy Materials, Xiamen University, 351005 Xiamen, P. R. China*

† Electronic supplementary information (ESI) available. See DOI: 10.1039/c8cp01840e

 This journal is © the Owner Societies 2018

Published on 25 April 2018. Downloaded by Tsinghua University on 6/28/2018 3:59:49 AM.

transport properties of three AsP can be attributed to the distinct low-frequency optical phonons associated with their chemical structures. Our findings highlight potential strategies for achieving enhanced thermoelectric efficiency of group VA materials *via* the alloying method.

2. Methods

2.1. Density functional theory calculation

The initial structure of single-layered AsP was constructed from the monolayer structure of puckered black phosphorus, and it was optimized using the Vienna ab initio simulation package (VASP) with the projector augmented wave (PAW) method and the Perdew–Burke–Ernzerhof (PBE) exchange–correlation functional.[27–29] We added a 20 Å vacuum in the out-of-plane direction to build a slab model for the monolayer AsP. A 600 eV cut-off for the plane-wave basis set was chosen, and the convergence criteria for the structural relaxation was set as the forces on each atom less than 0.005 eV $Å^{-1}$. The spin–orbit coupling effect was taken into account due to the heavy arsenic atoms in AsP. Since the band gap predicted by the PBE functional was usually underestimated, we re-calculated the band energies using the HSE06 hybrid functional.[30,31] The second-order interatomic force constants of the optimized structure were derived by utilizing the small-displacement and finite-differences method. With the help of symmetry operations, the number of displacements can be greatly reduced. Harmonic phonon properties, including phonon frequencies and phonon eigenvectors, were then obtained by diagonalizing the dynamical matrix using the Phonopy package.[32]

2.2. Thermal conductivity calculation

The lattice thermal conductivity κ can be derived from the classical molecular dynamics simulation. However, the results thus obtained rely heavily on the empirical potentials, which may not be sufficiently accurate. In this study, we have adopted a method based on the first-principles molecular dynamics (FPMD) to derive the phonon lifetime. In the FPMD, the potential used to describe interatomic interactions is obtained on-the-fly *via* the density functional theory.[33,34] Previous studies demonstrate that the lattice thermal conductivities predicted by this method agree well with the experimental data.[35,36]

In the theory of solid state, lattice thermal resistivity arises from phonon scatterings with other phonons, lattice defects, and grain boundaries. In the phonon lifetime approximation, the lattice thermal conductivity can be expressed as

$$\kappa = \sum_{s}^{3n} \int_{q} {\upsilon_{q,s}}^{2} c_{q,s} \tau_{q,s} \mathrm{d}q \qquad (1)$$

via a solution to the Boltzmann transport equation (BTE) for phonons. Herein, n is the number of atoms in the unit cell, $\upsilon_{q,s}$ is the phonon group velocity, $c_{q,s}$ is the heat capacity, and $\tau_{q,s}$ is the lifetime of the s-th phonon mode with the wave-vector q. The phonon group velocity and heat capacity can be obtained easily by performing the first-principles lattice dynamics calculation as described in Section 2.1.

To derive the phonon lifetime, we have followed the procedure illustrated in ref. 37, where more details of the formulation can be found. We used a 4 × 4 supercell for the FPMD simulation in VASP. A canonical ensemble (*NVT*) simulation of over 4 ps was first carried out to equilibrate atomic positions and velocities at room temperature. Subsequently, a microcanonical ensemble (*NVE*) simulation was performed for more than 35 ps to produce the time evolution in phase space, which was then used to evaluate the atomic-mass weighted velocity auto-correlation function. A Fourier transform of the velocity correlation function provides the phonon spectral energy density (SED), which represents the phonon energy in the frequency domain. Wherever the phonon lifetime approximation is valid, the velocity auto-correlation function can be written as a sum of $3n$ damped harmonic oscillators, and the phonon SED has a form of[35]

$$g(q,\nu) = \frac{1}{k_{\mathrm{B}}T} \sum_{s}^{3n} \frac{2I^{0}\tau_{q,s}}{1 + \left(2\pi\tau_{q,s}\left(\nu - \nu_{q,s}\right)\right)^{2}} \qquad (2)$$

We thus extracted the phonon lifetime $\tau_{q,s}$ from the linewidth of the phonon SED according to eqn (2). We chose the 75 × 75 q-mesh for the integral of eqn (1) after the convergence test.

3. Results and discussion

3.1. Geometry and electronic structure of AsP

The geometry of a single-layered AsP is presented in Fig. 1, which is similar to that of b-P and puckered arsenene. Herein, we built three possible chemical structures of AsP by replacing half of phosphorus atoms in the unit cell of b-P with arsenic atoms, denoted hereinafter as AsP-1, AsP-2, and AsP-3. There are in total two phosphorus atoms and two arsenic atoms in the unit cell of AsP, located respectively at two atomic layers. In AsP-1, only As–P bonds exist, both in-plane and out-of-plane. The top layer of AsP-2 is constituted exclusively by phosphorus atoms and the bottom layer is constituted by arsenic atoms; thus, AsP-2 is characterized by in-plane As–As and P–P bonds and out-of-plane As–P bonds. By contrast, there are in-plane As–P bonds and out-of-plane As–As and P–P bonds in AsP-3. The optimized geometric parameters are supplied in Table 1. Our results are very close to those obtained in previous studies, where charge transport properties of these three AsP structures have been calculated.[20,21,38] We have to point out that the nomenclatures for these structures may be different in the literature, for example, AsP-1, AsP-2, and AsP-3 herein are named α_3, α_2, and α_1, respectively in ref. 20.

Fig. 2 presents electronic band structures of three AsP allotropes along with that of b-P for comparison, and all these have been calculated at the HSE06 level of theory. Our results show that all of them are direct band gap semiconductors. Both valence band maximum (VBM) and conduction band minimum (CBM) are located at the Γ point, the center of the Brillouin zone. The band gaps of AsP-1, AsP-2, and AsP-3 are 1.51 eV, 1.45 eV, and 1.59 eV, respectively, as compared to 1.47 eV of b-P.

Published on 25 April 2018. Downloaded by Tsinghua University on 6/28/2018 3:59:49 AM.

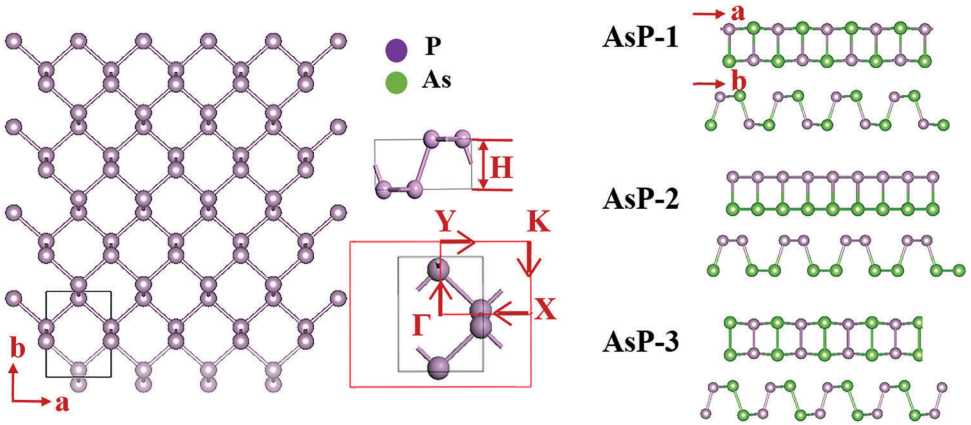

Fig. 1 Puckered structure of b-P and the first brillouin zone. Three AsP monolayers are built by substituting two of four phosphorous atoms in the unit cell of b-P with two arsenic atoms. the right panel shows the side view of three AsP structures along zigzag (a) and armchair (b) directions respectively. In AsP-1, there exist only As–P bonds. AsP-2 has in-plane As–As, P–P and out-of-plane As–P bonds. AsP-3 has in-plane As–P bonds and out-of-plane As–As and P–P bonds.

Table 1 Geometry paramters for b-P and three types of AsP. *a* and *b* are the unit cell parameters, *H* is the puckering height. X–X (in) and X–X (out) represent the in-plane and out-of-plane bond lengths (Å) respectively

		a/Å	*b*/Å	*H*/Å	P–P (in)	P–P (out)	As–As (in)	As–As (out)	As–P (in)	As–P (out)
b-P		3.35	4.43	2.12	2.23	2.25	—	—	—	—
AsP	1	3.51	4.65	2.36	—	—	—	—	2.38	2.38
	2	3.51	4.65	2.27	2.29	—	2.46	—	—	2.38
	3	3.51	4.65	2.39	—	2.22		2.53	2.38	—

The VBM and CBM of these three AsP are mainly constituted by the $3p_z$ orbital of phosphorus and $4p_z$ orbital of arsenic atoms with almost equal contributions, except for the CBM of AsP-3 where arsenic atoms contribute more. This leads to the larger band gap of AsP-3 because the $4p_z$ orbital of arsenic has higher energy than the $3p_z$ orbital of phosphorus. The smaller band gap of AsP-2 can be attributed to its smaller puckering height and lack of in-plane As–P bonds. Remarkably, the bandgaps of all three AsP fall perfectly in the range of 1.2–1.6 eV required for optimum light harvesting in solar cells.

3.2. Stabilities and phonon dispersion of AsP

The thermodynamic stabilities of AsP monolayers are examined by their cohesive energies and their phonon dispersion spectra.

The cohesive energy of AsP monolayers is defined as $E_{coh} = (2E_{As} + 2E_P - E_{Total})/4$, where E_{As}, E_P, and E_{Total} are the energies of an individual arsenic atom, an individual phosphorous atom, and a unit cell of AsP monolayers, respectively. The cohesive

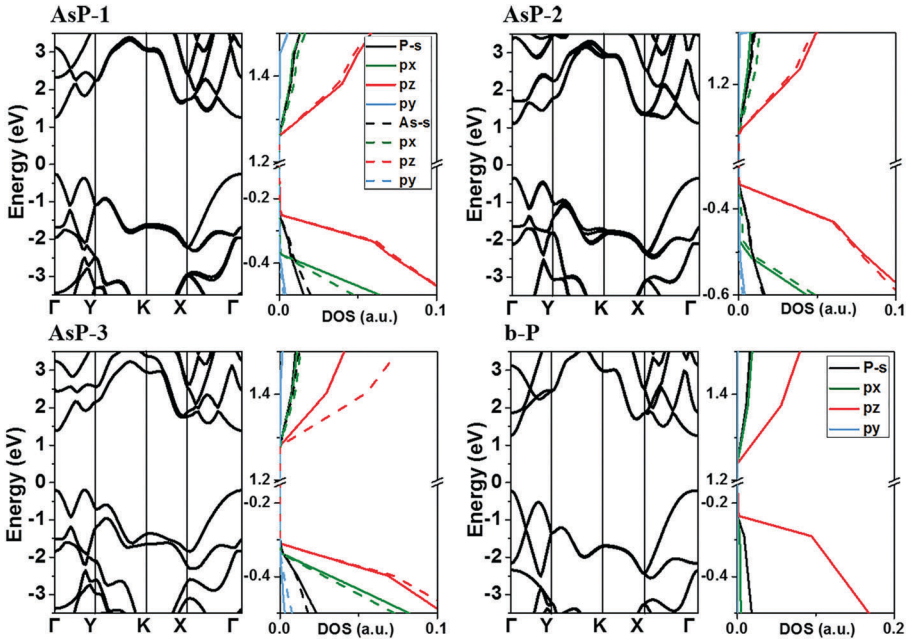

Fig. 2 Band structure and partial density of states for three types of AsP and b-P.

 This journal is © the Owner Societies 2018

Published on 25 April 2018. Downloaded by Tsinghua University on 6/28/2018 3:59:49 AM.

energies of three AsP monolayers are 3.15, 3.15, and 3.17 eV per atom. These values are slightly smaller than the cohesive energy of b-P (3.47 eV per atom calculated by us and 3.477 eV per atom reported in a previous study[39]), but larger than that of gray arsenic monolayer (2.84 eV per atom).[40] The result of cohesive energies also indicates that these three AsP structures are almost equally stable, and all of them may exist.

The thermal stability of AsP monolayer was also examined by the FPMD simulation. A 4 × 4 supercell was used in our simulation at room temperature (300 K). Fig. S1 (ESI†) shows the image of AsP monolayers at the end of 20 ps MD simulation. These images show that AsP monolayers can maintain their structural integrity throughout the simulation. These results reveal that AsP monolayers may have good thermal stability at room temperature. As observed from the As–P phase diagram, the melting point of $As_xP_{(1-x)}$ is around 900 K.[41] At 800 K, our FPMD simulation shows that the basic skeleton of AsP monolayer is retained although small deformations in the chemical bonds appear (Fig. S1, ESI†).

The kinetic stability of AsP monolayers is confirmed by their phonon dispersions along the high-symmetry directions in the irreducible Brillouin zone (BZ) (Fig. 3a–c). There is no appreciable imaginary frequency in the phonon dispersion curves; this implies good kinetic stability of the AsP monolayers. As compared to that of b-P (Fig. 3d), the phonon frequency of longitudinal acoustic (LA) modes at the boundary of BZ (*X*-point) decreases from 6.03 THz to 3.85 THz, 3.73 THz, and 3.78 THz due to the increased molecular weight of AsP. The acoustic modes, in the long wavelength limit, represent the whole translational motion of the unit cell; thus, the frequency is closely related to the total atomic mass in the cell. As a consequence, the dispersions of acoustic modes in all three AsP structures are really similar to each other (Table S1, ESI†), but those of the optical modes are profoundly different due to their distinct chemical structures and bonding characters. We have also analyzed the partial density of states (PDOS) of phonons on two types of atoms, *i.e.* As and P (Fig. 3). The DOS projected on phosphorous atoms is mainly located at high frequencies and that on arsenic atoms is located at low frequencies. This is determined by the different atomic masses of the two elements, *i.e.* 31 *versus* 75.

3.3. Lattice thermal conductivities of AsP

The lattice thermal conductivities of b-P and AsP are listed in Table 2. The thermal conductivity of b-P is 29.95 W m^{-1} K^{-1} and 14.13 W m^{-1} K^{-1} along the zigzag and armchair directions, respectively. Our results are in excellent agreement with those obtained previously, which are 30.15 W m^{-1} K^{-1} and 13.65 W m^{-1} K^{-1}, based on the first-principles third-order force constants method for the phonon scattering rate.[42] It should be noted that in our method, all the anharmonic effects, not limited to the three-phonon scatterings arising from third-order force constants, have been included. The thermal conductivities of three AsP structures, in both zigzag and armchair directions, are smaller than that of b-P. Moreover, the anisotropy of thermal conduction observed in b-P is preserved in AsP. As shown in Table 2, acoustic phonons contribute more than 50% to the total thermal conductivity, and three lowest-frequency optical phonons contribute around 15–30%. To unravel the cause of reduced thermal conductivities, we have listed phonon group velocities (v) and relaxation times (τ) of all the vibrational modes in b-P and AsP in Table S2 (ESI†). From the phonon dispersion

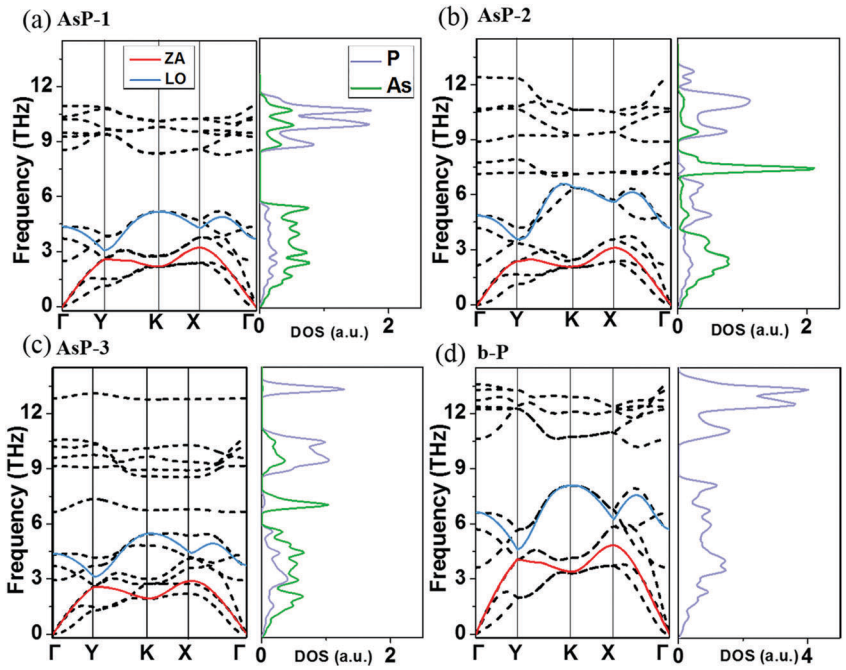

Fig. 3 Phonon dispersion and partial density of states for three types of AsP and b-P. black dashed lines represent the original dispersion, and colored solid lines are the dispersion with off-diagonal *xz* and *yz* components of the force constants turned off (ZA in red and LO in blue).

Published on 25 April 2018. Downloaded by Tsinghua University on 6/28/2018 3:59:49 AM.

Table 2 Thermal conductivities (W m^{-1} K^{-1}) in zigzag and armchair directions and anisotropy for three types of AsP as compared with b-P. The data in the last two rows are the heat transport contribution of acoustic phonon modes and low-frequency optical phonon modes, respectively

	AsP-1	AsP-2	AsP-3	b-P
κ (ZZ/AC)	10.97/4.19	26.30/6.42	11.50/3.69	29.95/14.13
Anisotropy	2.61	4.10	3.12	2.12
Acoustic (%)	64	53	67	64
Low-O (%)	21	25	16	32

curves shown in Fig. 3 and the data presented in Table S2 (ESI†), we can see that the group velocities of acoustic and low-frequency optical modes in b-P are twice as large as those in AsP. Although the change of phonon scattering rates (τ^{-1}) is not as evident, we attribute the reduced lattice thermal conductivities in AsP mainly to the decreased group velocities of phonons.

Thermal transport properties amongst these three allotropes of AsP are also profoundly different. The thermal conductivities of AsP-1, AsP-2, and AsP-3 are 10.97 W m^{-1} K^{-1}, 26.30 W m^{-1} K^{-1}, and 11.50 W m^{-1} K^{-1} in the zigzag direction and 4.19 W m^{-1} K^{-1}, 6.42 W m^{-1} K^{-1}, and 3.69 W m^{-1} K^{-1} in the armchair direction, respectively. Thus, AsP-2 possesses much larger thermal conductivity than the other two allotropes. The reason is analyzed as follows. The chemical structure of AsP-2 is distinct from that of the other two allotropes as arsenic atoms are located exclusively in one sub-layer and phosphorus atoms are located in the other; thus, the surface of AsP-2 is relatively smooth, lacking in-plane As–P bonds. The smaller puckering angle leads to the thinner AsP monolayer: the puckering height in AsP-2 is 2.27 Å, smaller than 2.36 Å in AsP-1 and 2.39 Å in AsP-3. More importantly, distinct bonding structures of AsP-2 lead to distinct phonon dispersion and scattering rates. As discussed at the beginning of this section, three acoustic and three lowest-frequency optical phonon modes contribute most to the thermal conductivity. Thus, we focused on these phonon modes. The dispersion relations of three acoustic modes, as shown in Fig. 3a–c, are nearly identical for the three AsP allotropes; this indicates almost the same group velocities, which is also confirmed by our calculated results listed in Table 3. However, the dispersion relations for the optical phonon modes are very different. The three lowest-frequency optical phonon modes are illustrated in Fig. S2 (ESI†). These are out-of-plane waving movement (ZO) and in-plane sliding movements (TO and LO) of sub-layers along the two perpendicular directions *a* and *b*. The total dispersion of the three optical modes is 4.7 THz in AsP-2, much larger than 2.7 THz and 2.9 THz in the other two allotropes; this indicates larger group velocities in the former. We tried to find the origin of this difference by analyzing the coupling between in-plane and out-of-plane vibrations. In puckered 2D materials, vibrations in the *xy*-plane (*ab*-plane) and *z*-direction (*c*-direction) hybridize. For example, in b-P with the puckered structure, both the *xz* and *yz* components of second-order force constants are non-zero,[43] whereas these terms vanish in graphene with a completely planar lattice. If we set all the *xz* and *yz* off-diagonal terms of second-order force constants in AsP and b-P to zero, the coupling between in-plane and out-of-plane vibrations will disappear. By comparing the original phonon dispersions (black dashed lines in Fig. 3) with those of the completely decoupled phonons (colored solid lines in Fig. 3), we conclude that the ZA–LO coupling in these puckered 2D materials leads to softening of the ZA mode and stiffening of the LO mode. It is different from that observed for buckled 2D materials, where both LO and TO modes have higher energies and the LA–ZO coupling is significant, leading to the formation of the acoustic-optical gap.[44] The ZA–LO phonon coupling in puckered AsP and b-P causes flattening of both phonon bands and reduced group velocities of phonons. Among all three AsP structures, the ZA–LO phonon coupling in AsP-2 is least because the As–As and P–P covalent bonds within each sub-layer are orthogonal to the *z*-direction; thus, the phonon group velocities in AsP-2 are largest.

Table 3 The phonon relaxation times (ps) and group velocities (km s^{-1}) of three acoustic modes (branch 1, 2 and 3) and three low-frequency optical modes (branch 4, 5 and 6) in AsP. γ is the average Grüneisen parameter of all phonon modes at the Γ-point

	AsP-1		AsP-2		AsP-3	
Branch	τ	v	τ	N	τ	v
1	13.6	1.38	14.2	1.39	17.2	1.32
2	13.1	1.19	26.2	1.25	11.8	1.47
3	10.5	1.77	33.9	1.62	13.8	1.73
4	9.12	1.56	21.5	1.44	8.86	1.20
5	8.06	1.54	12.6	1.81	5.98	1.24
6	6.01	0.94	8.04	2.65	5.52	1.00
γ	12.39		5.05		15.60	

In addition to harmonic phonon properties, phonon scatterings arising from the anharmonic effect also play an important role in thermal conduction. In the process of phonon scatterings, selection rules such as energy and momentum conservations should be obeyed. It is generally accepted that a large phonon gap between different modes would suppress phonon scattering channels. In AsP-2, the energy gap between LO/TO and ZO/LA/TA/ZA modes is larger at the *K*-point than that in the other two allotropes. Furthermore, Grüneisen parameters are widely used to describe the anharmonic interactions of phonons, defined as $\gamma_{q,s} = -[A/\omega_{q,s}][\mathrm{d}(\omega_{q,s})/\mathrm{d}A]$ for the monolayer structure, where A is the area of the unit cell and $\omega_{q,s}$ is the frequency of mode s at the q-point. The Grüneisen parameter at the Γ-point averaged over all phonon modes is 5.05 in AsP-2, which is significantly smaller than that in AsP-1 (12.39) and AsP-3 (15.60), indicating relatively small anharmonic effect in AsP-2. As a result, the phonon relaxation time of AsP-2 is about twice as large as that of the other two allotropes (Table 3). The velocity auto-correlation functions of the LA mode at the Γ-point are plotted in Fig. 4 for all three AsP allotropes, and that for AsP-2 apparently decays much slower than the other two; this indicates larger relaxation times. Overall, we could reasonably ascribe larger thermal conductivity of AsP-2 to its unique feature of bonding, which leads to low-frequency optical modes with higher group velocities, weak anharmonicity, and suppressed scattering channels.

This journal is © the Owner Societies 2018

Published on 25 April 2018. Downloaded by Tsinghua University on 6/28/2018 3:59:49 AM.

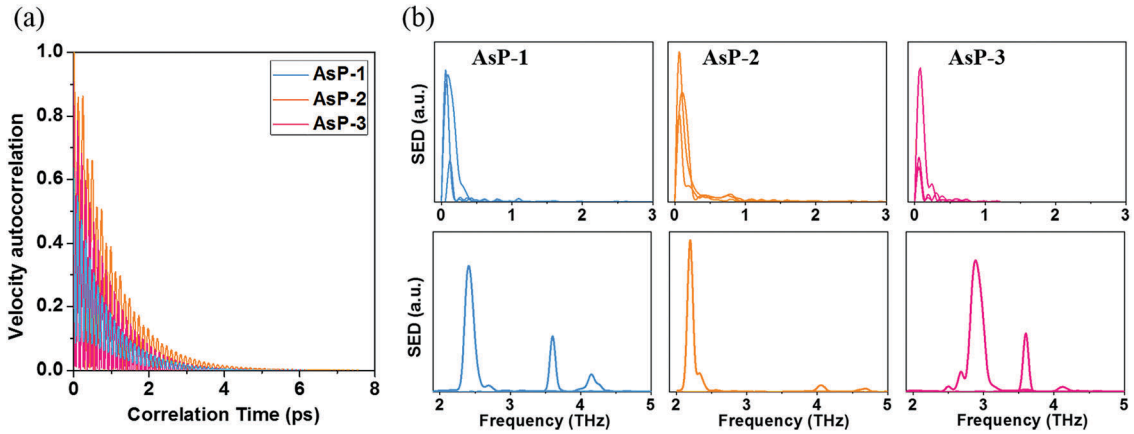

Fig. 4 (a) Velocity auto-correlation function of longitudinal acoustic (LA) mode at the γ-point for three types of AsP, with a 1 ps damping function. Compared with the other two allotropes, the decay time of AsP-2 is much longer, indicating larger phonon relaxation time. (b) Phonon spectral energy density (SED) at the Γ-point for three acoustic (upper panel) and three low-frequency optical (lower panel) phonon modes in AsP-1, AsP-2, and AsP-3, respectively. The phonon lifetimes can be extracted from the linewidths of these peaks.

4. Conclusion

In summary, we have investigated thermal transport properties of a puckered AsP monolayer, a new type of layered material of group-VA, based on the first-principles molecular dynamics. The phonon dispersion relation and high cohesive energy indicate that these compounds may be prepared in monolayers. We reveal that by substitution of phosphorous atoms with heavy arsenic atoms, thermal conductivities are significantly reduced; this can be attributed to the reduced phonon group velocities in AsP. Based on the larger charge mobilities predicted for AsP,[20,21] we propose that AsP may be a more promising thermoelectric material than b-P. Moreover, the profound anisotropy of thermal conduction in AsP indicates that it can be used for thermal modulation.

The thermal transport properties are significantly different for the three chemical structures of AsP. Among them, AsP-2 with the same type of elements lying in one sub-layer exhibits much higher thermal conductivity, which is mainly attributed to its unique low-frequency optical phonon modes. In AsP-2, these modes have larger group velocities, and the larger phonon gap further suppresses phonon scatterings; this leads to larger relaxation times of phonons. Our results highlight the importance of atomic arrangement in the thermal transport properties of AsP, and the structure–property relationship established may provide new thinking and guidance on the fabrication of thermoelectric materials by the engineered alloying method.

Conflicts of interest

The authors declare no competing financial interests.

Acknowledgements

This work was supported by the National Natural Science Foundation of China (Grant No. 21673123, 21290190, and 91333202) and the Ministry of Science and Technology of China (Grant No. 2015CB655002). Computational resources are provided by the Tsinghua Supercomputing Center.

Notes and references

1 K. S. Novoselov, A. K. Geim, S. V. Morozov, D. Jiang, Y. Zhang, S. V. Dubonos, I. V. Grigorieva and A. A. Firsov, *Science*, 2004, **306**, 666–669.
2 K. S. Novoselov, A. K. Geim, S. V. Morozov, D. Jiang, M. I. Katsnelson, I. V. Grigorieva, S. V. Dubonos and A. A. Firsov, *Nature*, 2005, **438**, 197–200.
3 Y. Zhang, Y. W. Tan, H. L. Stormer and P. Kim, *Nature*, 2005, **438**, 201–204.
4 K. S. Novoselov, D. Jiang, F. Schedin, T. J. Booth, V. V. Khotkevich, S. V. Morozov and A. K. Geim, *Proc. Natl. Acad. Sci. U. S. A.*, 2005, **102**, 10451–10453.
5 B. Radisavljevic, A. Radenovic, J. Brivio, V. Giacometti and A. Kis, *Nat. Nanotechnol.*, 2011, **6**, 147–150.
6 A. Splendiani, L. Sun, Y. Zhang, T. Li, J. Kim, C. Chim, G. Galli and F. Wang, *Nano Lett.*, 2010, **10**, 1271–1275.
7 Q. H. Wang, K. Kalantar-Zadeh, A. Kis, J. N. Coleman and M. S. Strano, *Nat. Nanotechnol.*, 2012, **7**, 699–712.
8 S. Zhang, M. Xie, F. Li, Z. Yan, Y. Li, E. Kan, W. Liu, Z. Chen and H. Zeng, *Angew. Chem., Int. Ed.*, 2016, **55**, 1666–1669.
9 H. J. Liu, A. T. Neal, Z. Zhu, Z. Luo, X. Xu, D. Tomanek and P. D. Ye, *ACS Nano*, 2014, **8**, 4033–4041.
10 F. Xia, H. Wang and Y. Jia, *Nat. Commun.*, 2014, **5**, 4458.
11 S. Zhang, Z. Yan, Y. Li, Z. Chen and H. Zeng, *Angew. Chem., Int. Ed.*, 2015, **54**, 3112–3115.
12 Z. Y. Zhang, H. N. Cao, J. C. Zhang, Y. H. Wang, D. S. Xue and M. S. Si, *AIP Adv.*, 2015, **5**, 067117.
13 C. Kamal and M. Ezawa, *Phys. Rev. B: Condens. Matter Mater. Phys.*, 2015, **91**, 085423.
14 J. Qiao, X. Kong, Z. X. Hu, F. Yang and W. Ji, *Nat. Commun.*, 2014, **5**, 4475.

Published on 25 April 2018. Downloaded by Tsinghua University on 6/28/2018 3:59:49 AM.

15 Y. Wang and Y. Ding, *Nanoscale Res. Lett.*, 2015, **10**, 254.
16 Y. Sun, D. Wang and Z. Shuai, *J. Phys. Chem. C*, 2017, **121**, 19080–19086.
17 Y. Zhao, Y. Chen, Y. Zhang and S. Liu, *Mater. Chem. Phys.*, 2017, **189**, 215–229.
18 Z. Yang, J. Hao, S. Yuan, S. Lin, H. M. Yau, J. Dai and S. P. Lau, *Adv. Mater.*, 2015, **27**, 3748–3754.
19 I. Shirotani, J. Mikami, T. Adachi, Y. Katayama, K. Tsuji, H. Kawamura, O. Shimomura and T. Nakajima, *Phys. Rev. B: Condens. Matter Mater. Phys.*, 1994, **50**, 16274–16278.
20 F. Shojaei and H. S. Kang, *J. Phys. Chem. C*, 2015, **119**, 20210–20216.
21 M. Xie, S. Zhang, B. Cai, Y. Huang, Y. Zou, B. Guo, Y. Gu and H. Zeng, *Nano Energy*, 2016, **28**, 433–439.
22 D. M. Rowe, V. S. Shukla and N. Savvide, *Nature*, 1981, **290**, 765–766.
23 S. Lee, K. Esfarjani, J. Mendoza, M. S. Dresselhaus and G. Chen, *Phys. Rev. B: Condens. Matter Mater. Phys.*, 2014, **89**, 085206.
24 R. Cheaito, J. C. Duda, T. E. Beechem, K. Hattar, J. F. Ihlefeld, D. L. Medlin, M. A. Rodriguez, M. J. Campion, E. S. Piekos and P. E. Hopkins, *Phys. Rev. Lett.*, 2012, **109**, 195901.
25 Z. Zhu, J. Guan and D. Tomanek, *Nano Lett.*, 2015, **15**, 6042–6046.
26 B. Liu, M. Kopf, A. N. Abbas, X. Wang, Q. Guo, Y. Jia, F. Xia, R. Weihrich, F. Bachhuber, F. Pielnhofer, H. Wang, R. Dhall, S. B. Cronin, M. Ge, X. Fang, T. Nilges and C. Zhou, *Adv. Mater.*, 2015, **27**, 4423–4429.
27 J. P. Perdew and Y. Wang, *Phys. Rev. B: Condens. Matter Mater. Phys.*, 1992, **45**, 13244–13249.
28 G. Kresse and J. Furthmuller, *Phys. Rev. B: Condens. Matter Mater. Phys.*, 1996, **54**, 11169–11186.
29 G. Kresse and D. Joubert, *Phys. Rev. B: Condens. Matter Mater. Phys.*, 1999, **39**, 1758–1775.
30 J. Heyd, G. E. Scuseria and M. Ernzerhof, *J. Chem. Phys.*, 2003, **118**, 8207–8215.
31 J. Heyd, G. E. Scuseria and M. Ernzerhof, *J. Chem. Phys.*, 2006, **124**, 219906.
32 A. Togo, F. Oba and I. Tanaka, *Phys. Rev. B: Condens. Matter Mater. Phys.*, 2008, **78**, 134106.
33 P. E. Blöchl and M. Parrinello, *Phys. Rev. B: Condens. Matter Mater. Phys.*, 1992, **45**, 9413–9416.
34 D. M. Bylander and L. Kleinman, *Phys. Rev. B: Condens. Matter Mater. Phys.*, 1992, **46**, 13756–13761.
35 N. de Koker, *Phys. Rev. Lett.*, 2009, **103**, 125902.
36 Y. Lu, T. Sun, P. Zhang, P. Zhang, D. B. Zhang and R. M. Wentzcovitch, *Phys. Rev. Lett.*, 2017, **118**, 145702.
37 J. A. Thomas, J. E. Turney, R. M. Iutzi, C. H. Amon and A. J. H. McGaughey, *Phys. Rev. B: Condens. Matter Mater. Phys.*, 2010, **81**, 081411.
38 J. Sun, N. Lin, H. Ren, C. Tang, L. Yang and X. Zhao, *Phys. Chem. Chem. Phys.*, 2016, **18**, 9779–9787.
39 Y. Zhang, Z. F. Wu, P. F. Gao, D. Q. Fang, E. H. Zhang and S. L. Zhang, *Phys. Chem. Chem. Phys.*, 2017, **19**, 2245–2251.
40 Z. Zhu, J. Guan and D. Tomanek, *Phys. Rev. B: Condens. Matter Mater. Phys.*, 2015, **91**, 161404.
41 I. Karakaya and W. T. Thompson, *J. Phase Equilib.*, 1991, **12**, 343–346.
42 G. Qin, Q. B. Yan, Z. Qin, S. Y. Yue, M. Hu and G. Su, *Phys. Chem. Chem. Phys.*, 2015, **17**, 4854–4858.
43 C. Li and Z. Tian, *Nanoscale Microscale Thermophys. Eng.*, 2017, **21**, 45–57.
44 B. Peng, D. Zhang, H. Zhang, H. Shao, G. Ni, Y. Zhu and H. Zhu, *Nanoscale*, 2017, **9**, 7397–7407.

 This journal is © the Owner Societies 2018